NASA
Technical Memorandum 83640

AVRADCOM
Technical Report 84-C-6

Comparison Between Measured Turbine Stage Performance and the Predicted Performance Using Quasi-3D Flow and Boundary Layer Analyses

Robert J. Boyle
Lewis Research Center
Cleveland, Ohio

and

Jeffrey E. Haas
Propulsion Laboratory
AVRADCOM Research and Technology Laboratories
Lewis Research Center
Cleveland, Ohio

and

Theodore Katsanis
Lewis Research Center
Cleveland, Ohio

Prepared for the
Twentieth Joint Propulsion Conference
cosponsored by the AIAA, SAE, and ASME
Cincinnati, Ohio, June 11-13, 1984

NASA

U.S. ARMY AVRADCOM

COMPARISON BETWEEN MEASURED TURBINE STAGE PERFORMANCE AND THE PREDICTED PERFORMANCE USING QUASI-3D FLOW AND BOUNDARY LAYER ANALYSES

by

Robert J. Boyle
National Aeronautics and Space Administration
Lewis Research Center
Cleveland, Ohio 44135

Jeffrey E. Haas
Propulsion Laboratory
AVRADCOM Research and Technology Laboratories
National Aeronautics and Space Administration
Lewis Research Center
Cleveland, Ohio 44135

and

Theodore Katsanis
National Aeronautics and Space Administration
Lewis Research Center
Cleveland, Ohio 44135

E-2065

Abstract

A method for calculating turbine stage performance is described. The usefulness of the method is demonstrated by comparing measured and predicted efficiencies for nine different stages. Comparisons are made over a range of turbine pressure ratios and rotor speeds. A quasi-3D flow analysis is used to account for complex passage geometries. Boundary layer analyses are done to account for losses due to friction. Empirical loss models are used to account for incidence, secondary flow, disc windage, and clearance losses.

Nomenclature

C	parameter in profile loss calculation
C_l	rotor clearance, fraction of span
C_w	coefficient in disc windage loss model
C_1	coefficient used in Eq. (1)
C_2	coefficient used in Eq. (1)
c	chord, m
c_p	specific heat, J/kg•K
D	parameter in profile loss calculation
$\bar{e}$	kinetic energy loss coefficient
f	friction factor
g	gap between rotor disc and stationary surface, m
h	blade height, m
i	incidence (gas minus blade) angle
L	kinetic energy loss, J/kg
$\dot{m}$	flow rate, kg/sec
P	pressure, N/m^2
p	exponent used in Eq. (1)
r	radius, m
Re	Reynolds number
R_r	rotor reaction
s	pitchwise distance between blades, m
T	temperature, K
V	absolute velocity, m/sec
W	relative velocity for rotor, absolute velocity for stator, m/sec
x	axial distance between rotor and measuring station, m
Y	loss coefficient $\frac{P_{o1} - P_{o2}}{P_{o2} - P_2}$
Z	blade loading coefficient $4(\tan \alpha_1 - \tan \alpha_2)^2 \frac{\cos^2 \alpha_2}{\cos \alpha_m}$
α_1	inlet air angle
α_2	exit air angle
α_m	mean air angle $\tan^{-1}\left(\frac{\tan \alpha_1 + \tan \alpha_2}{2}\right)$
β_1	inlet blade angle
γ	specific heat ratio
δ_1	displacement thickness
δ_{te}	blade trailing edge thickness, m
η	efficiency
θ	momentum thickness, m
μ	viscosity, m-sec/kg
ρ	density, kg/m^3
ψ	kinetic energy thickness, m
Ω	pitchwise angle
Ω_p	angular distance for one pitch
ω	speed of rotation, rad/sec

Subscripts

oa	overall
cL	clearance
cr	critical velocity
d	rotor disc
e	endwall
ex	exhaust duct
fs	free stream
h	hub
i	incidence
m	mixed out location
o	total (absolute for stators, relative for rotors)
p	profile
rot	rotor
s	secondary
st	stator
t	tip
w	windage

0 zero clearance
1 inlet to blade row
2 exit of blade row

Superscripts

* normalized by pitchwise distance
' absolute total
" relative total

Introduction

In the effort to improve turbine performance greater use is being made of complex blade passage geometries.[1-3] These geometries can include contoured endwalls, and blades that are leaned and bowed, resulting in nonuniform work distributions. A method for predicting turbine stage performance has been developed which accounts for the effects of complex passage geometries. The method uses a quasi-3D inviscid flow analysis iteratively coupled to calculated losses so that changes in losses result in changes in the flow distribution. In this manner the effects of both the geometry on the flow distribution and the flow distribution on losses are accounted for in the prediction of stage performance. This report consists of a description of the method, and a comparison between predicted and measured stage performance for nine different single stage axial turbines. The turbines had diameters between 12 and 75 cm, and design pressure ratios between 1.8 and 3.1. The present method was developed primarily as an aid in understanding why a particular stage performs as it does. The reason for undertaking this effort is that existing correlations[4-6] do not account for all geometric factors which affect stage performance. This work is an extension of the work described in Ref. 7 which was used to predict the change in stator performance due to endwall contouring.

The analysis uses a quasi-3D flow analysis coupled to a boundary layer analysis to determine losses due to friction on the blade surfaces and passage endwalls. The flow analysis assumes inviscid flow, and uses existing programs.[8,9] The boundary layer analysis also uses an existing program.[10] The profile losses for both the stator and rotor are determined by using the results of the boundary layer analysis along with flow and geometry information in the loss model of Ref. 11. Empirical models are used to account for incidence, disc cavity, rotor tip clearance, and secondary vortex losses. In order to demonstrate the validity of the method, comparisons are made between predicted and measured stage efficiencies over a range of pressure ratios and rotor speeds for each of the nine turbines. A range of operating conditions was examined for each turbine in order to assess the adequacy of the individual loss models. For example, decreasing speed at constant pressure ratio increases rotor incidence loss. The ability of the analysis to predict the change in efficiency when speed is reduced is a measure of the adequacy of the incidence loss model. The adequacy of the tip clearance model is assessed by comparing predicted and experimental stage efficiencies at different rotor clearances for a single turbine. In addition to stage efficiencies the analysis provides other data of interest to a designer. Comparisons are made between predicted and experimental flow angles for three turbines at their design conditions.

Method of Analysis

The predicted stage performance was calculated by first determining the stator performance. These results determined the flow field entering the rotor. After the rotor performance was determined, the overall stage performance was then calculated. For each blade row the flow field was determined using a quasi-3D flow analysis. This analysis was done using existing stream function flow analysis codes. First a hub-to-shroud solution was obtained using the program MERIDL described in Ref. 8. One of the results of the MERIDL calculation is the variation of stream-sheet thickness with streamwise location for various spanwise locations. The stream-sheet thickness is the thickness necessary to pass a fixed fraction (one percent in this program) of the total flow. These results and other data were used as input to obtain the blade-to-blade solution. This solution was obtained using the program TSONIC described in Ref. 9. The flow conditions at the exit of the blade row were not imposed as part of the input. They were iterated until the static pressure near the trailing edge was the same for both the pressure and suction surfaces of the blade.

The flow analysis was done using modified versions of the MERIDL and TSONIC programs. Modifications to the program MERIDL are described in Appendix A, and TSONIC contained the modifications of Ref. 12. These modifications allowed solutions to be obtained in the transonic flow regime. However, the presence of shocks was not accounted for. Appendix A also describes two additional modifications made to TSONIC. One allows blade-to-blade solutions to be obtained assuming trailing edge ejection of sufficient flow to give no velocity defect behind the trailing edge. The second modification allows the specification of an elliptical blade leading edge in the program TSONIC. These two modifications are presented to document the current status of the program, but were not used in the subject investigation.

Once the flow analysis was done for the stator row, boundary layer analyses were performed. These analyses were done along streamline paths for both the blade surfaces and endwalls. The analyses were done using the program BLAYER described in Ref. 10. Boundary layer parameters were obtained along streamline paths determined from the inviscid analysis. The profile loss was calculated using the method of Ref. 11, and the endwall loss using the method of Ref. 7. Appendix B gives a summary of the equations used to determine losses, and shows how these values were used to determine stage efficiency. The loss in total pressure used in the flow analyses could be a function of span. To do so requires assumptions regarding the spanwise distribution of loss. The simplest assumption was that there was no spanwise variation, and this assumption was used for most of the comparisons. After the losses for the stator were determined they were compared with the assumed values used in the flow analysis. If there was a difference new losses were assumed for use in the flow analysis and the analysis was

repeated. This is shown in Fig. 1 which is a block diagram of the procedure used to determine stage efficiency.

Once the losses for the stator row had been determined, the process was repeated for the rotor using the results of the stator analysis as input to the rotor analysis. The procedure for calculating losses was the same for the rotor as for the stator, with the losses being calculated in the relative frame. Only hub friction losses were calculated for the rotor, since the tip friction loss would be included as part of the tip clearance loss. The duct loss is the loss due to friction on the endwalls between the rotor trailing edge and the measuring station. A friction coefficient was used as a simplified boundary layer analysis to determine this loss. This was done primarily as a convenience, since the program BLAYER could have been used to determine this loss.

The losses due to incidence, windage, and clearance are summarized in Ref. 13. The incidence loss is based on the assumption that the kinetic energy in the normal component of velocity is lost. The actual equations used for incidence loss incorporate the empirical results of Ref. 14. The results of Ref. 14 give a six degree bias in the zero loss incidence angle, and a greater loss for positive incidence. The disc windage loss accounted for the friction between the rotating disc and stationary surfaces. The equations of Ref. 15 were used. This loss was not applied to those stages where the disc windage loss was included as part of the tare loss. The loss resulting from the clearance between the rotor tip and the casing used the data of Ref. 16. The change in stage efficiency due to clearance is a function of the rotor gap and rotor reaction. The equations used to express this functional relationship are the same as those given in Ref. 17.

The calculations were carried out on an IBM 370 computer. Approximately 3 min of CPU time were needed to converge a case for each blade row.

Secondary loss model. The correlation for the loss due to the secondary vortex was the only loss correlation which was modified for the present analysis. There are two widely quoted secondary loss correlations. These are Morris and Hoare,[18] and Dunham.[19] The equations are of a similar form and both can be expressed as:

$$Y_s = Z \frac{\cos \alpha_2}{\cos \beta_1} \left(\frac{c}{h}\right) \left[C_1 \left(\frac{\delta_1}{c}\right)^p + C_2\right] \qquad (1)$$

For the correlation of Morris and Hoare $C_1 = 0.294$, $C_2 = 0.011$, and $p = 1.0$. For Dunhams's correlation $C_1 = 0.078$, $C_2 = 0.055$, and $p = 0.5$. The secondary loss is the sum of two terms. The first term is a function of the inlet boundary layer height, and represents the loss resulting from the formation of the leading edge vortex. The second term is loss due to boundary layer growth on the endwall. This is the same loss as is accounted for by endwall boundary layer growth calculated by the BLAYER analysis. The endwall loss is strongly dependent on the distance between the trailing edge and the measuring station. Neither correlation accounts for variations in this parameter, while the endwall boundary layer analysis did. Therefore, the secondary loss model used herein was only the first term of Eq. (1). The question of the appropriate coefficients for this term remained to be resolved. Figure 2 shows a comparison of the two correlations, along with the experimental data that was used for the correlation of Dunham. The total loss values for both correlations are in good agreement. However, they differ significantly for the loss due only to the inlet boundary layer. The equation of Morris and Hoare gives nearly a lower bound for the loss due to the inlet boundary layer. Also shown in Fig. 2 is a curve for the loss due to the inlet boundary layer that is 1.5 times that of Morris and Hoare. It is in better agreement with the data for those cases where the experimental loss either did not or may not have included the endwall loss. Coefficients of $C_1 = 0.44$, $C_2 = 0$, and $p = 1.0$ were chosen for the secondary loss. The equation used for the secondary loss due to the inlet boundary layer is 1.5 times the value used by Morris and Hoare, and is:

$$Y_s = Z \frac{\cos \alpha_2}{\cos \beta_1} \left(\frac{c}{h}\right) 0.44 \left(\frac{\delta_1}{c}\right) \qquad (2)$$

The secondary loss model was then used to compare predicted and measured kinetic energy loss coefficients for three stators. Table I gives this comparison for experimental data from Ref. 20. These stators were later used in stage tests, and the experimental data for the stage tests will be discussed subsequently. The data are for stators 13 cm in diameter, which have cylindrical, conical, and S-shaped contoured tip endwalls. This table shows a breakdown of the analytic losses for the three stators. The secondary loss due just to the inlet boundary layer is approximately one quarter of the total loss for all three stators. The ratio of the total wall displacement thicknesses to the blade chord at the blade leading edge varied between 0.008 and 0.013. It can be seen from Fig. 2 that this is in a region where the correlation of Dunham and the correlation of Morris and Hoare for the secondary loss due to the inlet boundary layer significantly disagree. The agreement between the analysis and the measured data is good because the secondary loss was chosen as 1.5 times the value from the correlation of Morris and Hoare. Also, a preliminary screening of the data for the nine turbines showed that the unmodified equation of Morris and Hoare led to a higher than measured efficiency, while the equation of Dunham led to a lower than measured efficiency.

Comparisons With Experimental Data

Stage descriptions. Some characteristics of the nine axial flow turbines are shown in Table II. The individual stages are labeled according to their tip diameter. A wide range of turbine sizes is represented. With one exception all of the stages were tested with an inlet temperature near ambient, and that one had an inlet temperature of only 422 K. The tests were run with either the inlet or exit pressure near atmospheric. The stages are ordered according to their equivalent flow. Some stages had common blade rows. Stage 42A and 42B had the same stator, but different rotors. This was also true of stages

25U and 25T. These last two turbines differed in that the untwisted rotor of 25U was twisted for turbine 25T. Stages 13-Cyl and 13-Cone had different stators, but the same rotor. Turbine 13-Cyl had cylindrical stator endwalls, while 13-Cone had a conical tip endwall.

Stage efficiency comparisons. Figures 3 to 11 give comparisons of the predicted and measured stage efficiency for the nine stages. In each figure data are given for three speeds, between 80 and 110% of equivalent design speed. For each stage the analysis was able to predict the efficiency within 1.2 points at design pressure ratio and speed. Off-design comparisons were made for each of the nine turbines at constant work factor, which is near the operating line. These comparisons are shown in table III. Some turbines do not have comparisons at off-design speeds, because there was no experimental data available at the required pressure ratio. With the exception of turbine 51 at 80% speed, the analysis was able to predict the efficiencies within 2 points.

Table IV gives comparisons between measured and predicted efficiencies at each design pressure ratio for each speed. The analysis was able to predict the efficiencies at off-design speeds about as well as it did at 100% speed. At 100% speed the analysis overpredicted the stage efficiency by an average of 0.2 point. At 110% speed the average overprediction was also 0.2 point. At 90% speed the average overprediction was 0.4 point, but there were only three comparisons. At 80% speed the average overprediction was 0.1 point. When the rotor speed is varied, but the pressure ratio is held constant, there are significant changes in the loss due to incidence. Other losses also change, but to a lesser extent. The results of the comparisons in table IV indicate that the incidence loss model is reasonably accurate.

Figures 3 to 11 show that as the pressure ratio is decreased at constant rotor speed there was a greater discrepancy between the analysis and the experimental data. This is a result of the procedure used for the blade boundary layer calculations. When separation was indicated, the surface velocities were smoothed until the calculation went as far as the trailing edge. For many of the rotors, pressure surface separation was indicated at low pressure ratios. For example, at pressure ratios less than 2.2 the analysis showed separated boundary layers at all speeds for turbine 51. The analysis showed separated boundary layers, but could not predict the penalty associated with the separation. If the penalty could be predicted, the efficiency would be lower than the efficiency predicted with a smoothed velocity profile. For each of the nine turbines predictions are shown for pressure ratios greater than the design pressure ratio. The agreement with the experimental data is about as good as it was at the design pressure ratio. The predictions do not cover the entire pressure range for all turbines. The analytic predictions were made only in the region where the rotor exit Mach number was less than 1.3. Shock loss would be significant only at higher Mach numbers. Turbines 25U and 25T show a rapid decrease in experimental efficiency at the highest pressure ratios. This may have been the result of shock losses.

Clearance effects. Figure 12 shows stage efficiency versus rotor clearance for turbine 13-Cyl at design speed. Results are shown at both constant work and constant pressure ratio. In each case two predictions are shown. One prediction assumes rotor loss is uniformly distributed from hub to tip. The other prediction has a linear loss distribution. In this second prediction losses other than tip clearance loss are uniformly distributed. The tip clearance loss varies linearly, with none of the loss at the hub and the average loss at mid-span. The turbine had a relatively large design clearance of 2.4% of span. At the design clearance both loss distribution assumptions result in the same efficiency. The difference between the predicted efficiencies for the two loss distribution assumptions increases with increased clearance. Even the uniform loss distribution model gives a satisfactory prediction for the change in efficiency with clearance.

Loss breakdown. Figure 13 shows the breakdown of losses for the different turbines at the design point. The individual losses are normalized by the overall loss, so that they are a fraction of the total loss. The effect of turbine size can be seen from the data in this figure. The 25 cm turbines and the 13 cm turbines both had clearances of nearly 2.5% of span. For the 25 cm turbines the clearance loss is about half the total loss for the stage, while for the 13 cm turbines it is only about a third of the total loss. Also evident is the growth of the importance of rotor secondary flow loss as the size decreased. The rotor secondary loss is large because of the large amount of flow turning and the thickness of the inlet boundary layer. In reference to Fig. 2, the total inlet boundary layer displacement thickness for turbine 13-Cyl was only 0.01 of the rotor chord. This turbine has the largest loss due to rotor secondary flow of the nine turbines. At this value there is a large difference between the correlation of Morris and Hoare and the correlation of Dunham for the secondary loss due to the presence of the endwall boundary layer at the blade leading edge. The rotor secondary loss is an uncertain loss. Added to the uncertainty arising from the cascade data is the uncertainty arising from skewing of the rotor inlet boundary layer. A 50% variation in the rotor secondary vortex loss would account for most of the difference between the predicted and experimental efficiencies.

Flow angles. A comparison between measured rotor exit flow angles and flow angles predicted by the analysis is given in Fig. 14. The comparison are for turbines 12, 13-Cyl, and 13-Cone at the design condition. Viscous effects play a significant role in determining the local flow angle. The predictions are reasonably good considering that the analysis has no spanwise variation in loss, and that the flow angles were determined from the quasi-3D inviscid flow analysis.

Concluding Remarks

A method for predicting turbine stage performance has been developed. This method uses a quasi-3D inviscid flow analysis iteratively coupled to calculated losses to predict stage performance. At the design pressure ratio and

speed it was able to predict the stage efficiency within 1.2 points. The agreement was not as good at other conditions. Near the operating line the analysis was generally able to predict the efficiency within 2.0 points. At low pressure ratios and design speed the analysis generally predicted a significantly higher efficiency than was measured. The analysis indicated when separation was likely to occur, but proceeded to smooth the surface velocities until no separation occurred. This was done before the loss prediction was made. For the cases where separation occurred, it could be inferred that the actual efficiency would be less than predicted. Because of the high losses associated with separated flow it is desirable to be better able to predict the condition at which separation begins, and to be able to calculate the losses when separation occurs. To improve the precision in determining when separation occurs, if it occurs near the leading edge, a blade-to-blade solver such as described in Ref. 26 would be useful. This program determines a more accurate solution in the leading edge region through the use of body fitted coordinates. In order to better define profile loss at other than design conditions, a method of calculating loss with a separated boundary layer would be desirable. However, this was beyond the scope of this work.

The analysis predicted stage efficiencies at high pressure ratios reasonably well. The analysis was not used in regions where shock losses would be significant. Use of flow analyses which would account for these losses, as well as directly accounting for viscous losses, would increase confidence in the model. However, use of codes which incorporated these features would have resulted in much larger computational times. This in turn would have lessened the number of cases for which comparisons could be made.

Appendix A - Description of Modifications to the Programs MERDIL and TSONIC

Trailing Edge Ejection. One of the difficulties in using the TSONIC program[9] is determining the outlet flow angle, BETAO. (This appendix uses the nomenclature of Refs. 8, 8a, and 9.) If the trailing edge was sharp, there would be no difficulty, since the Kutta condition could be used. However, on real turbomachines blades, there is considerable thickness at the trailing edge. The usual practice has been to visually examine the velocities near the trailing edge on the suction and pressure surfaces, and then to adjust BETAO until the velocities on the two surfaces approach a common value at the trailing edge. This usually requires good judgement because of the velocity peaks induced by the flow going around the small trailing edge radius. An alternative scheme has been devised, whereby the trailing edge radius may be replaced by a blunt trailing edge. Because of the large blockage, and to avoid flow around a sharp corner, flow is considered to be issuing from the trailing edge at the average velocity of the freestream flow between the blades at the trailing edge. This also has the effect of compensating for wake blockage downstream of the blades.

The blade configuration at the trailing-edge should have a small uniform curvature near the trailing edge with a moderate wedge angle (see Fig. 15). If the wedge angle is small the velocities will vary smoothly near the trailing edge. With a larger wedge angle there will tend to be a reduced surface velocity at the trailing edge. In either case the trailing edge velocities will vary smoothly with a variation of BETAO. This makes its feasible to write coding to vary either the downstream whirl or BETAO to obtain closure of the suction and pressure surface velocities.

Four subroutines are affected by the changes required to simulate trailing edge flow ejection. First, the blade geometry is modified to have a blunt trailing edge. This is done in BLCD. Then, because of the additional mass flow from the trailing edge, the downstream periodic boundary condition is changed to allow for the increased mass flow. This requires changes to subroutines COSUB and VELSUB. Another change that is required is to provide for proper boundary values along the blunt trailing edge (see Fig. 15). This requires changes to COSUB and VELTAN.

Figure 15 shows the geometry of the blunt trailing edge as derived from the original trailing edge radius. The tangent line to the trailing edge radius is extended to the trailing edge as shown in Fig. 15. The equation for the distance from the center of the trailing edge to the intersection point is

$$q = R_o \left(\frac{\pm 1 + \sin \beta}{\cos \beta} \right) \qquad (A1)$$

The coordinates of this intersection point is used for the last spline point on the blade, and replaces the spline point at the tangent point on the trailing edge radius.

Figure 15 also shows the mesh geometry at the trailing edge. Additional flow comes out the trailing edge. It is assumed that the ejection velocity is the average velocity across the passage at the trailing edge. The stream function (u) varies from zero to 1 from the lower blade to the upper blade. Then the stream function increases linearly across the blunt trailing edge of the upper blade. The total increase is equal to the tangential blade thickness divided by the tangential passage width at the trailing edge.

Elliptical Leading or Trailing Edges. The TSONIC program uses subroutine BLCD to calculate the blade geometry. The version of BLCD published in Ref. 9 uses circular arcs at the leading and trailing edges. This is satisfactory for many blades, however, in some cases it is not. One way to obtain a more general leading edge shape is to use an ellipse which may be at an angle. The only subroutine changed is BLCD. The input format was not changed, but the definitions of several input variables were changed. The new definitions are given in Table V, and are illustrated in Fig. 16. See Ref. 9 for the input format. The equation of an ellipse at an angle, BETI1, to the x-axis is:

$$y = \frac{Cx \pm RI1 * RI2 \sqrt{A - x^2}}{A} \qquad (A2)$$

where

$$A = RI1^2 \cos^2(BETI1) + RI2^2 \sin^2(BETI1)$$
$$C = \sin(BETI1) \cos(BETI1) (RI1^2 - RI2^2)$$

The maximum and minimum value of x is $\pm\sqrt{A}$. The corresponding value of y is Cx/A. Therefore:

$$x_{min} = -\sqrt{A}, \quad \text{at} \quad y = -\frac{C}{\sqrt{A}}$$
$$x_{max} = \sqrt{A}, \quad \text{at} \quad y = \frac{C}{\sqrt{A}} \tag{A3}$$

Equations (A2) and (A3) are used in BLCD to calculate the θ coordinate of the blade surface for any given m-coordinate, using $y + C/\sqrt{A} = r\theta$, and $x + \sqrt{A} = m$ on the ellipse.

Mesh Generation for MERIDL. The MERIDL program[8] generates an orthogonal mesh, which is used to obtain a finite difference solution to the stream function equation. The scheme for generating the solution mesh is described in Ref. 8a. After generating the streamwise mesh lines, the hub-to-shroud mesh lines are generated to be orthogonal to the streamwise mesh lines. The hub is divided into equal increments within the blade, and upstream and downstream of the blade. In some cases with high wall curvature, this can result in crowding of the hub-to-shroud mesh lines in some region, and wide distances between lines in another region. This can be alleviated somewhat by starting at a streamwise mesh line near a region of high curvature. Figure 17 shows the grids generated using different starting locations. When the grid is uniform at mid-span, the grid is widely spaced in the region of high curvature. When the grid is started two lines away from the curved wall, the spacing is better at this wall, and not too compressed at the opposite wall. The only subroutine that is affected is MESHO. The revised subroutine starts at the middle of the passage and goes both directions. The index of the initial streamwise mesh line is JMID. JMID can be set to any value from 1 to MHTP1, (the mesh line at the tip), to determine the starting line for generating the hub-to-shroud mesh lines.

Alternate Method for Calculating Tangential Velocity Components. The basic MERIDL program uses an empirical correction to the blade shape near the leading and trailing edges. This is done to avoid a discontinuity in tangential momentum when there is nonzero incidence or deviation angles. The empirical correction is described Appendix F of Ref. 8. The correction, however, is not satisfactory in many cases. It is particularly poor in cases with low solidity (1/2 or less). In some cases with low solidity, the flow does not become parallel to the blade surface anywhere in the passage. An alternate scheme was devised to improve the calculations for cases with very low solidity. Instead of using the blade geometry angles directly, the tangential momentum is used. The tangential momentum upstream and downstream of the blade is specified as a function of the stream function. For the new scheme the tangential momentum within the blade passage is assumed to vary in proportion to the variation of the tangent of the streamwise blade angle. If the passage height varies by less than 50% between the leading and trailing edges, the effect on the BESP array used by TSONIC is not large.

There is an additional advantage to specifying the tangential momentum instead of the blade angle within the blade. When the blade angle is specified, the stream function equation becomes hyperbolic when the relative velocity becomes supersonic on the mean stream surface. If the velocity becomes supersonic anywhere within the blade on the stream surface, MERIDL cannot calculate the solution. However, when the tangential momentum is specified, the stream function equation does not become hyperbolic until the meridional component of the relative velocity becomes supersonic. Normally, the meridional component of the velocity will be subsonic, even with supersonic relative velocity, so that a solution can be obtained.

Two subroutines were changed and a new subroutine (TANVEL) was added to calculate the tangential velocity components. The velocity components are calculated by NEWRHO. In the original version, W_θ is calculated from the meridional components W_s and W_t by using the blade slopes, $d\theta/ds$ and $d\theta/dt$. The alternate method calculates W_θ by varying the whirl (rV_θ) in the same manner as the variation in $rd\theta/ds$ between the leading and trailing edges. This calculation is done by TANVEL, which is called by NEWRHO. The rest of NEWRHO is essentially unchanged. In addition INDEV was changed to eliminate the calculation of $d\theta/ds$ near the leading and trailing edges.

Appendix B - Summary of Equations Used In Loss Model

This appendix describes the equations used to calculate losses which are in turn used to calculate stage efficiency. These equations are specifically for an axial machine. However, the loss calculation is implemented in a general way, and the performance of a radial stage can be calculated using the method described in Ref. 27.

Profile Loss. - The profile loss is calculated according to the method of Stewart.[12] It includes the effects of boundary layer growth along the blade surfaces as well as the thickness of the blade trailing edge (station 1). The profile loss is calculated at a location where complete mixing is assumed to have occurred (station m). The velocity and total pressure are uniform in the pitchwise direction. To calculate the kinetic loss coefficient two parameters (C and D) are first calculated:

$$C = \frac{1 - \frac{\gamma-1}{\gamma+1}\left(\frac{W}{W_{cr}}\right)^2_{fs,1}\left(\frac{\gamma+1}{2\gamma}\right) + \cos^2\alpha_2(1 - \delta^* - \delta^*_{te} - \theta^*)\left(\frac{W}{W_{cr}}\right)^2_{fs,1}}{\cos\alpha_1\,(1 - \delta^* - \delta^*_{te})\left(\frac{W}{W_{cr}}\right)_{fs,1}}$$

$$D = \left(\frac{W}{W_{cr}}\right)_{fs,1} \sin\alpha_2 \; \frac{1 - \delta^*_{te} - \delta^* - r^*}{1 - \delta^* - \delta^*_{te}}$$

where δ^* is a normalized displacement thickness

$$\delta^* = \frac{\delta_{1,s} + \delta_{1,p}}{s\cos\alpha_2}$$

where $\delta_{1,s}$ and $\delta_{1,p}$ are the displacement thickness on the suction and pressure surfaces near the trailing edge. Values are obtained from the boundary layer analysis which terminated one grid line upstream of the trailing edge. Similarly,

$$\theta^* = \frac{\theta_{1,s} + \theta_{1,p}}{s \cos \alpha_2} \quad \text{and} \quad \delta^*_{te} = \frac{\delta_{te}}{s \cos \alpha_2}$$

where δ_{te} is the blade thickness normal to the chamber line. The ratio of the component of velocity in the streamwise direction to the critical velocity $(W_x/W_{cr})_m$ is found from:

$$\left(\frac{W_x}{W_{cr}}\right)_m = \frac{\gamma C}{\gamma + 1} - \sqrt{\left(\frac{\gamma C}{\gamma + 1}\right)^2 - 1 + \left(\frac{\gamma - 1}{\gamma + 1}\right) D^2}$$

The density ratio $(\rho/\rho_o)_m$ is calculated from:

$$\frac{\rho}{\rho_{om}} = \left\{1 - \frac{\gamma - 1}{\gamma + 1}\left[D^2 + \left(\frac{W_x}{W_{cr}}\right)_m^2\right]\right\}^{\frac{1}{\gamma - 1}}$$

The total pressure ratio is calculated from

$$\frac{P_{om}}{P_{ol}} = \frac{\left(\frac{\rho}{\rho_o}\right)\left(\frac{W}{W_{cr}}\right)_{fs,1} \cos \alpha_1 (1 - \delta^* - \delta^*_{te})}{\left(\frac{\rho}{\rho_o}\frac{W_x}{W_{cr}}\right)_m}$$

The profile kinetic energy loss coefficient is calculated from:

$$\bar{e}_p = \frac{\left(\frac{P_{ol}}{P_{om}}\right)^{\frac{\gamma-1}{\gamma}} - 1}{\left(\frac{P_{ol}}{P_m}\right)^{\frac{\gamma-1}{\gamma}} - 1}$$

where,

$$\frac{P_{ol}}{P_m} = \frac{P_{ol}}{P_{om}}\frac{P_{om}}{P_m} \quad \text{with} \quad \frac{P_o}{P_m} = \left(\frac{\rho_{om}}{\rho_m}\right)^{\gamma}$$

The mass average profile loss for the entire passage is:

$$\bar{\bar{e}}_p = \frac{\int_{r_h}^{r_t} \rho W_x \bar{e}_p r \, dr}{\int_{r_h}^{r_t} \rho W_x r \, dr} \qquad \text{(B1)}$$

Endwall Loss - The endwall loss is determined from boundary layer calculations. The boundary layer growth is calculated for a number of inviscid streamlines in the blade passage. For the stator the streamlines extend from the upstream boundary to the rotor leading edge along both the hub at tip. For the rotor only boundary layer growth along the hub between the leading and trailing edges is considered. The endwall loss, derived in Ref. 7, is:

$$\bar{e}_e = \frac{\int_0^{\theta_p} [(\rho r \rho_{fs} W_{fs}^3 \cos \alpha)_h + (\rho r \rho_{fs} W_{fs}^3 \cos \alpha)_t] d\theta}{\int_0^{\theta_p}\left[\int_{r_h}^{r_t} r \rho_{fs} W_{fs}^3 \cos \alpha \, dr - (\delta r \rho_{fs} W_{fs}^3 \cos \alpha)_h - (\delta r \rho_{fs} W_{fs}^3 \cos \alpha)_t\right] d\theta} \qquad \text{(B2)}$$

Secondary Loss - The secondary loss is calculated for the inlet boundary layer on each endwall using equation 1. This equation does not account for any variation in free stream properties across the span. To account for the variation in an annular cascade a mass average of the secondary loss is done using the inviscid flow properties between the hub and tip. This results in:

$$\bar{Y}_s = \frac{\left[(Y_s \rho_{fs} W_{fs} \cos \alpha r)_h + (Y_s \rho_{fs} W_{fs} \cos \alpha r)_t\right] h}{\int_{r_h}^{r_t} r \rho_{fs} W_{fs} \cos \alpha \, dr} \qquad \text{(B3)}$$

From the definition of Y the equivalent $\bar{e}_s$ can be calculated.

Incidence Loss - The kinetic loss due to incidence is given in Ref. 14 as:

$$L_i = \frac{W_i^2}{2}[1 - \cos^n (i - i_{opt})]$$

where $i_{opt} = -6^o$ and $n = 3$ if $i > i_{opt}$ and $n = 2$ if $i < i_{opt}$. This is converted into an equivalent temperature drop, which in turn is converted into an $\bar{e}_i$ which represents a loss in total pressure due to incidence.

$$\bar{e}_i = \frac{L_i}{c_p T_{ol}}\left[1 - \left(\frac{P_{ol}}{P_2}\right)^{\frac{1-\gamma}{\gamma}}\right]^{-1}$$

Tip clearance Loss - The correlation for the tip clearance loss requires that the stage efficiency at zero clearance (η_0) be known. The ratio of stage efficiency to the efficiency at zero clearance is:

$$\frac{\eta}{\eta_0} = 1 - C_1 (1.72 + 0.108 R_r + 2.755 R_r^2)$$

C_1 is the clearance fraction and R_r is defined as:

$$R_r = \left(\frac{W_2^2 - W_1^2}{W_2^2 - W_1^2 + V_1^2}\right)_{tip}$$

Exhaust Duct Loss - The loss accounts for the pressure drop between the rotor exit and the measuring section

$\Delta P_{ex} = \frac{4f}{2(r_t - r_h)} \frac{x}{\cos\alpha} \frac{\rho_{ex} V_{ex}^2}{2}$, where f is the friction factor for a smooth tube at the exhaust

duct Reynolds number, the flow path length is $x/\cos\alpha$, and the hydraulic diameter is $2(r_t - r_h)$.

Disc Windage Loss - The rotor disc windage loss is given is Ref. 15 as:

$(Re)_d = \frac{\omega r_d^2 \rho_d}{\mu}$, where ω = rotor angular velocity, r_d = the disc radius, μ is the dynamic viscosity, and ρ_d is the average density at the hub. The loss coefficient is a function of the gap (g) and the Reynolds number.

$$C_w = 0.102 \left(\frac{g}{r_d}\right)^{-0.1} (Re)_d^{-0.2} \text{ if } (Re)_d \geq 1x10^5$$

$$C_w = 0.080 \left(\frac{g}{r_d}\right)^{-0.167} (Re)_d^{-0.25} \text{ if } (Re)_d < 1x10^5$$

The disc friction power loss is:

$$L_w = \frac{C_w \rho \omega^3 r_d^5}{2\dot{m}}$$

The equivalent kinetic energy loss coefficient is:

$$\bar{e}_w = \frac{L_w}{c_p T_1''} \left[1 - \left(\frac{P_1''}{P_2}\right)^{\frac{1-\gamma}{\gamma}}\right] -1$$

Stage Efficiency - The stator kinetic energy loss coefficient ($\bar{e}_{st}$) is taken as the sum of the loss coefficients for the stator. The rotor kinetic energy loss coefficient at zero clearance ($\bar{e}_{rot,0}$) is taken as the sum of the rotor kinetic loss coefficients for the incidence loss, profile loss, endwall loss, secondary loss, and disc windage loss. The stage efficiency is calculated in three steps. First the efficiency at zero clearance between the stator inlet and rotor exit is determined. Second, the change in efficiency due to rotor clearance is determined using equation B5. Third the overall stage efficiency is calculated by including the pressure drop in the exhaust duct. Figure 18 is a sketch of the paths followed in calculating the stage efficiencies. $P_1' - P_2'$ is the loss in total pressure in the stator. $P_2'' - P_3''$ is the loss in total pressure in the rotor excluding the clearance loss, while $P_2'' - P_4''$ includes the clearance loss. $P_4' - P_5'$ is the loss in total pressure in the exhaust duct. The zero clearance efficiency is:

$$\eta_0 = \frac{T_1' - T_{4,0}'}{(T_1' - T_{4,0}')_{id}} = \frac{1 - \frac{T_{4,0}'}{T_1'}}{1 - \left(\frac{P_4'}{P_1'}\right)^{\frac{\gamma-1}{\gamma}}}$$

$$= \frac{1 - \left(\frac{P_4'}{P_4''}\right)^{\frac{\gamma-1}{\gamma}} \left(\frac{P_2''}{P_2'}\right)^{\frac{\gamma-1}{\gamma}}}{1 - \left(\frac{P_4'}{P_1'}\right)^{\frac{\gamma-1}{\gamma}}}$$

and,

$$\frac{P_4'}{P_4''}\frac{P_2''}{P_2'} = \frac{P_4'}{P_1'}\frac{P_1'}{P_2'}\frac{P_2''}{P_4''}$$

The pressure ratios can be expressed in terms of stator and rotor kinetic energy loss coefficients.

$$\left(\frac{P_1'}{P_2'}\right)^{\frac{\gamma-1}{\gamma}} = 1 - \bar{e}_{st} + \bar{e}_{st}\left(\frac{P_1'}{P_2}\right)^{\frac{\gamma-1}{\gamma}}$$

$$\left(\frac{P_2''}{P_4''}\right)^{\frac{\gamma-1}{\gamma}} = 1 - \bar{e}_{rot,0} + \bar{e}_{rot,0}\left(\frac{P_2''}{P_4''}\right)^{\frac{\gamma-1}{\gamma}}$$

Then,

$$\eta_0 = \frac{1 - \left(\frac{P_4'}{P_1'}\right)^{\frac{\gamma-1}{\gamma}} \left[\left(1 - \bar{e}_{st} + \bar{e}_{st}\left(\frac{P_1'}{P_2'}\right)^{\frac{\gamma-1}{\gamma}}\right)\left(1 - \bar{e}_{rot,0} + \bar{e}_{rot,0}\left(\frac{P_2''}{P_4''}\right)^{\frac{\gamma-1}{\gamma}}\right)\right]}{1 - \left(\frac{P_4'}{P_1'}\right)^{\frac{\gamma-1}{\gamma}}} \quad (B7)$$

The efficiency including clearance is calculated from equation B5 to give:

$$\eta_{cL} = \eta_0 - \Delta\eta_{cL}$$

Since there is no additional work, but there is a pressure drop in the duct.

$$\eta_{oa} = \eta_{cL} \frac{1 - \left(\frac{P_4'}{P_1'}\right)^{\frac{\gamma-1}{\gamma}}}{1 - \left(\frac{P_5'}{P_1'}\right)^{\frac{\gamma-1}{\gamma}}}$$

References

1. Due, H. F.,Jr., Rogo, C., Kosier, C. L., and Jasas, G. B., "Advanced Small Axial Turbine Technology," USAAMRDL-TR-77-1, May 1977.

2. Ewen, J. S., Huber, F. W., and Mitchell, J. P., "Investigation of the Aerodynamic Performance of Small Axial Turbines," ASME Paper 73-GT-3, Apr. 1973.

3. "Low-Aspect-Ratio Turbine Technology Program," Aireasearch Manufacturing Co. Report 75-211701(2), Mar. 1977.

4. Ainley, D. G., and Mathieson, G. C. R., "A Method of Performance Estimation for Axial-Flow Turbines," ARC R & M 2974, 1951.

5. Craig, H. R. M., and Cox, H. J. A., "Performance Estimation of Axial Flow Turbines," Proceedings of the Institution of Mechanical Engineers, Vol. 185, No. 18, pp 407-424, 1971.

6. Kacker, S.C., and Okapuu, U., "A Mean Line Prediction Method for Axial Flow Turbine Efficiency," ASME Paper 81-GT-58, Mar. 1981.

7. Boyle, R. J., and Haas, J. E., "Comparison of Experimental and Analytic Performance for Contoured Endwall Stators," AIAA Paper 82-1286 June 1982.

8. Katsanis, T., and McNally, W. D., "Revised Fortran Program for Calculating Velocities and Streamlines on the Hub-Shroud Midchannel Stream Surface of an Axial-, Radial-, or Mixed-Flow Turbomachine or Annular Duct, Vol. I - User's Manual," NASA TN D-8430, 1977.

8a Katsanis, T., and McNally, W. D., "Revised Fortran Program for Calculating Velocities and Streamlines on the Hub-Shroud Midchannel Stream Surface of an Axial-, Radial-, or Mixed-Flow Turbomachine or Annular Duct, Vol. II - Programmer's Manual," NASA TN D-8431, 1977.

9. Katsanis, T., "Fortran Program for Calculating Transonic Velocities on a Blade-to-Blade Stream Surface of a Turbomachine," NASA TN D-5427, 1969.

10. McNally, W. D., "Fortran Program for Calculating Compressible Laminar and Turbulent Boundary Layers in Arbitrary Pressure Gradients," NASA TN D-5681, 1970.

11. Stewart, W. L., "Analysis of Two-Dimensional Compressible-Flow Loss Characteristics Downstream of Turbomachine Blade Rows in Terms of Basic Boundary-Layer Characteristics," NACA TN-3515, 1955.

12. Wood, J. R., "Improved Method for Calculating Transonic Velocities on Blade-to-Blade Stream Surfaces of a Turbomachine," NASA TP-1772, 1981.

13. Glassman, A. J., ed., "Turbine Design and Application," Vol. II, NASA SP-290, 1973.

14. Flagg, E. E., "Analytical Procedure and Computer Program for Determining the Off-Design Performance of Axial-Flow Turbines," NASA CR-710, 1967.

15. Daily, J. W., Ernst, W. D., and Asbedian, V. V., "Enclosed Rotating Disks with Superposed Throughflow-Mean Study and Periodic Unsteady Characteristics of the Induced Flow," Massachusetts Institute of Technology, Rep. R-64-16, Apr. 1964.

16. Hong, Y. S, and Groh, F.G., "Axial Turbine Loss Analysis and Efficiency Prediction Method," Boeing Co., Rep. D4-3220, Mar. 1966.

17. Jenkins, R.M., "A Comprehensive Method for Preliminary Design Optimization of Axial Gas Turbine Stages," AIAA Paper 82-1264, June 1982.

18. Morris, A. W. H., and Hoare, R. G., "Secondary Loss Measurements in a Cascade of Turbine Blades with Meriodional Wall Profiling," ASME Paper 75-WA/GT-13, Nov. 1975.

19. Dunham, J., "A Review of Cascade Data on Secondary Losses in Turbines," Journal of Mechanical Engineering Science, Vol. 12, Feb. 1970, pp 48-59

20. Haas, J. E., "Analytical and Experimental Investigation of Stator Endwall Contouring in a Small Axial-Flow Turbine, I -Stator Performance," NASA TP-2023, 1982.

21. Whitney, W. J, Szanca, E. M., Bider, B., and Monroe, D. E., "Cold-Air Investigation of a Turbine for High-Temperature-Engine Application, III - Overall Stage Performance," NASA TN D-4389, 1968.

22. Stabe, R. G., Whitney, W. J., and Moffitt, T. P., "Performance of a High-Work, Low Aspect Ratio Turbine Tested with a Realistic Inlet Radial Temperature Profile," AIAA Paper 84-1161, June 1984.

23. Szanca, E. M., Schum H. J., and Hotz, G. M., "Research Turbine for High-Temperature Core Engine Application. I - Cold Air Overall Performance of Solid Scaled Turbine," NASA TN D-7557, 1974.

24. Roelke, R. J., and Haas, J. E., "Cold-Air Performance of Compressor-Drive Turbine of Department of Energy Upgraded Automobile Gas Turbine Engine." NASA TM-83627, 1984.

25. Haas, J. E, and Boyle, R. J., "Analytical and Experimental Investigation of Stator Endwall Contouring in a Small Axial-Flow Turbine II -Stage Results," NASA TP-2309, 1984.

26. McFarland, E. R., "Solution of Plane Cascade Flow Using Improved Surface Singularity Methods," NASA TM-81589, 1981.

27. Civinskas, K. C. and Povinelli, L. A., "Application of a Quasi-3D Inviscid Flow and Boundary Layer Analysis to the Hub-Shroud Contouring of a Radial Turbine." AIAA Paper 84-1297, June 1984.

TABLE I. - COMPARISON OF MEASURED AND PREDICTED STATOR KINETIC ENERGY LOSS COEFFICIENTS FOR THREE 13 cm DIAMETER STATORS

	Kinetic energy loss coefficients ($\bar{e}_{st}$)		
	Stator		
	13-Cyl	13-Cone	13-S shaped
Predicted			
Profile	0.027	0.024	0.025
Endwall	.017	.016	.016
Secondary	.010	.011	.010
Incidence	.001	.001	.001
Total	.055	.052	.052
Measured[20]	0.055	0.052	0.052

TABLE II. - TURBINE CHARACTERISTICS AT THE DESIGN CONDITION

Label	Turbine								
	76 cm	51 cm	42-U	42-T	25-U	25-T	12 cm	13-Cyl	13-Cone
Tip diameter, cm.	76	51	42	42	25	25	12	13	13
Hub/Shroud radius ratio	0.75	0.86	0.85	0.85	0.85	0.85	0.73	0.83	0.81
Mean radius Reynolds no. ($\times 10^{-5}$)	2.7	8.1	8.4	8.4	8.7	8.7	2.4	3.1	3.1
Inlet total pressure, atm	1.0	3.1	1.0	1.0	1.7	1.7	0.8	1.4	1.4
Inlet total temperature, K	300	422	294	294	306	306	326	323	323
Stator									
Axial aspect ratio	2.4	1.0	1.0	1.0	1.0	1.0	1.0	0.7	0.7
Axial solidity	1.0	0.6	0.6	0.6	1.1	1.1	1.6	2.0	1.9
Pressure ratio - P_1'/P_2	1.5	1.9	1.9	1.9	1.6	1.6	1.6	2.0	2.0
Rotor									
Axial aspect ratio	1.9	1.1	1.0	1.0	1.1	1.1	1.2	0.5	0.5
Axial solidity	1.6	1.1	1.4	1.4	1.5	1.5	2.0	1.7	1.7
Rotor speed, rpm	4650	9048	10 686	10 686	12 750	12 750	29 440	33 300	33 300
Clearance, % span	0.75	0.80	0.86	0.86	2.30	2.30	1.20	2.40	2.40
Stage									
Total-to-total pressure ratio	1.75	2.72	3.1	3.1	1.82	1.82	2.05	2.77	2.77
Reference for experimental data	21	22	3	3	23	23	24	25	25

TABLE III. - COMPARISON BETWEEN MEASURED AND PREDICTED EFFICIENCIES AT CONSTANT WORK FACTOR

	Turbine								
	76	51	42 A	42 B	25 U	25 T	12	13-Cyl	13-Cone
% equivalent speed	100	100	100	100	100	100	100	100	100
Total-to-total pressure ratio	1.75	2.36	3.09	3.09	1.82	1.82	2.05	2.77	2.77
Measured efficiency	.922	.895	.920	.911	.874	.882	.863	.845	.855
Predicted efficiency	.923	.907	.916	.915	.881	.876	.865	.850	.853
% equivalent speed	90	110	110	110	110	110	110	110	110
Total-to-total pressure ratio	1.57	2.91			2.10	2.10			
Measured efficiency	.914	.895	N.A	N.A	.885	.894	N.A	N.A	N.A
Predicted efficiency	.913	.911			.879	.881			
% equivalent speed	80	80	90	90	80	80	80	80	80
Total-to-total pressure ratio	1.42	1.71	2.45	2.41	1.45	1.45	1.57		
Measured efficiency	.919	.857	.894	.900	.865	.890	.857	N.A	N.A
Predicted efficiency	.917	.888	.905	.908	.874	.883	.851		

TABLE IV. - COMPARISON BETWEEN MEASURED AND PREDICTED EFFICIENCIES AT DESIGN TEST PRESSURE RATIO

	Turbine								
	76	51	42 A	42 B	25 U	25 T	12	13-Cyl	13-Cone
% equivalent speed	100	100	100	100	100	100	100	100	100
Measured efficiency	.922	.895	.920	.911	.874	.882	.863	.845	.855
Predicted efficiency	.923	.907	.916	.915	.881	.876	.865	.850	.853
% equivalent speed	90	110	110	110	110	110	110	110	110
Measured efficiency	.904	.901	.921	.912	.884	.892	.876	.857	.863
Predicted efficiency	.900	.923	.919	.910	.878	.890	.877	.861	.865
% equivalent speed	80	80	90	90	80	80	80	80	80
Measured efficiency	.884	.845	.906	.901	.836	.860	.821	.799	.808
Predicted efficiency	.869	.848	.902	.913	.840	.845	.825	.795	.804

TABLE V. - NEW DEFINITIONS OF INPUT VARIABLES FOR ELLIPTICAL LEADING AND TRAILING EDGES

RI1 Semi-major axis of leading-edge ellipse

RI2 Semi-minor axis of leading-edge ellipse

BETI1
Angle of major axis of leading-edge ellipse.

BETI2
Not used

MSP1(1)
m-coordinate of tangent point of spline curve on leading-edge ellipse for upper surface (Surface 1). Previously not required.

MSP2(1)
Same as MSP1(1), but for lower surface (Surface 2).

RO1 Semi-major axis of trailing edge ellipse

RO2 Semi-minor axis of trailing edge ellipse

BETO1
Angle of major axis of trailing edge ellipse

BETO2
Not used

MSP1(SPLNO1)
Same as MSP1(1), but at trailing edge

MSP2(SPLNO2)
Same as MSP1(SPLNO1), but for lower surface

Note: If the trailing edge is circular, but the leading edge is elliptical, it is necessary to specify that the values of MSP1(SPLNO1) and MSP2(SPLNO2).

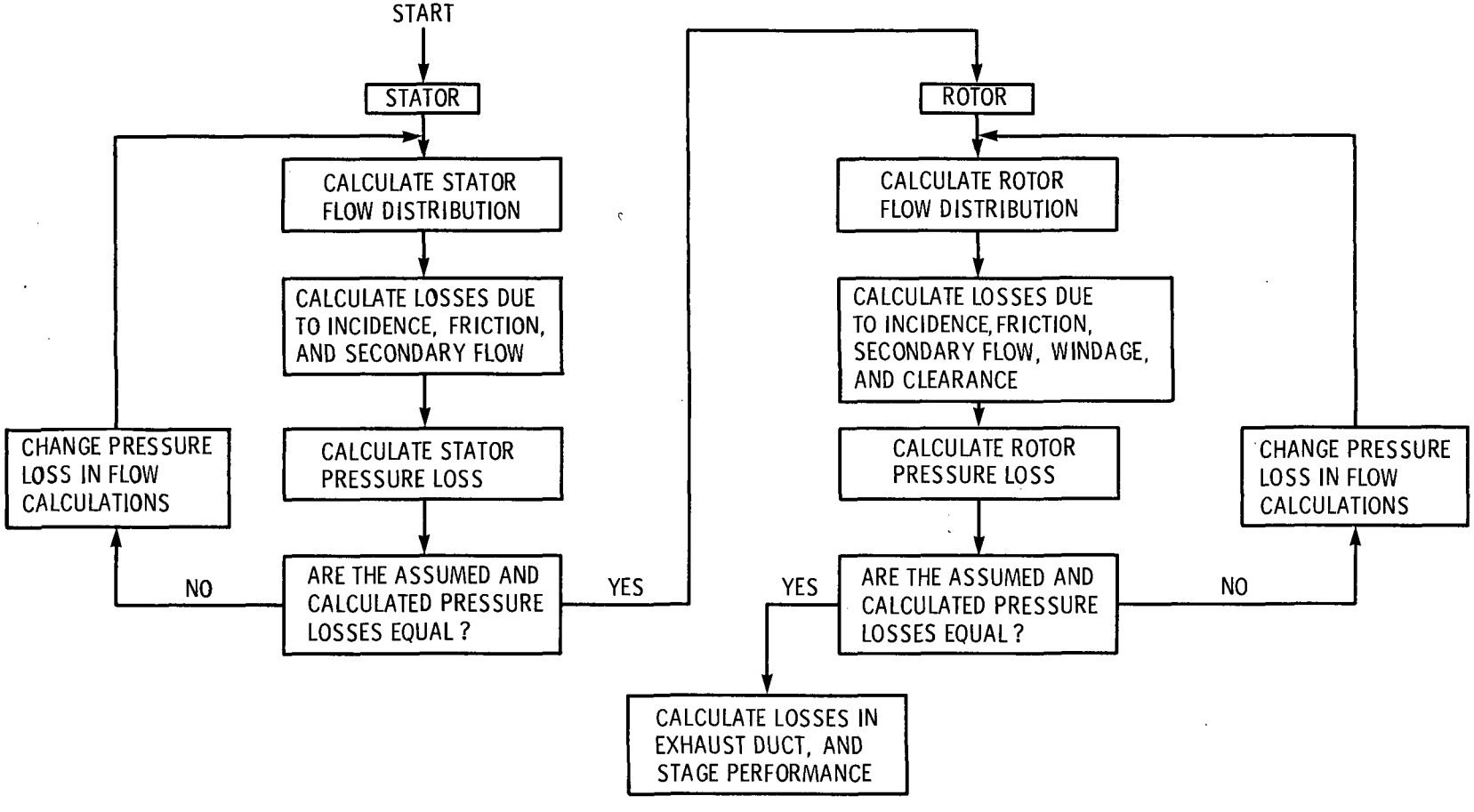

Figure 1. - Diagram of procedure used to calculate stage efficiency.

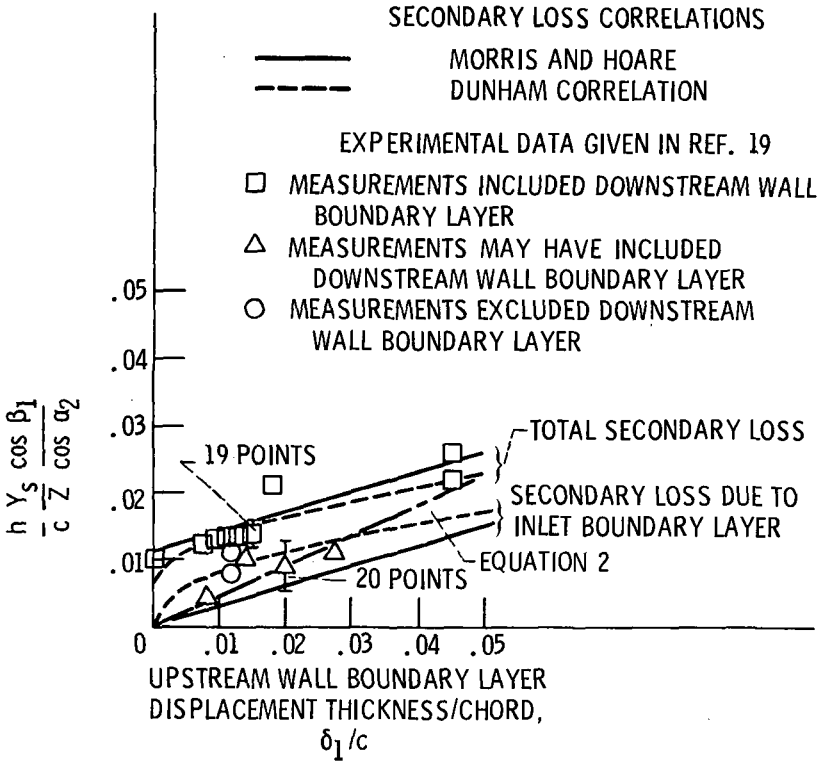

Figure 2. - Comparison of secondary loss correlations with the experimental data given in reference 19.

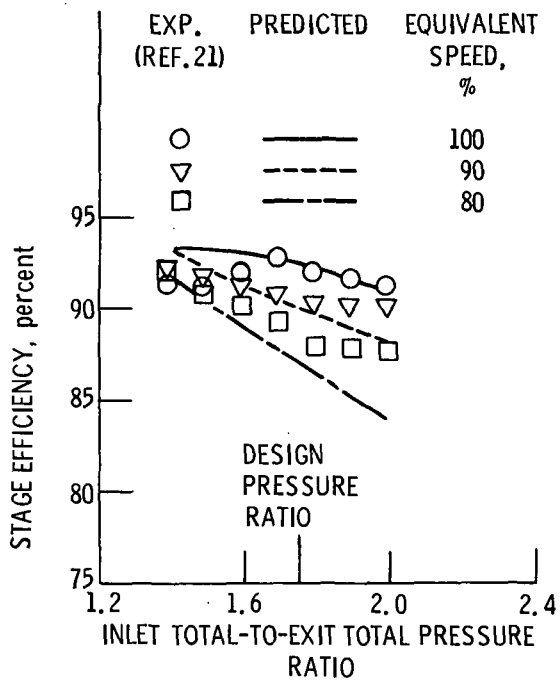

Figure 3. - Comparison of measured and predicted efficiencies for stage 76.

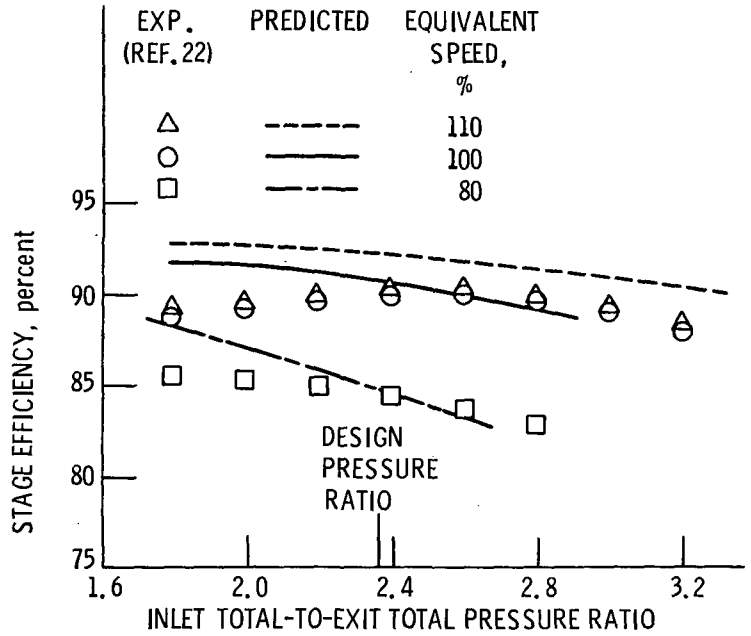

Figure 4. - Comparison of measured and predicted stage efficiency for stage 51.

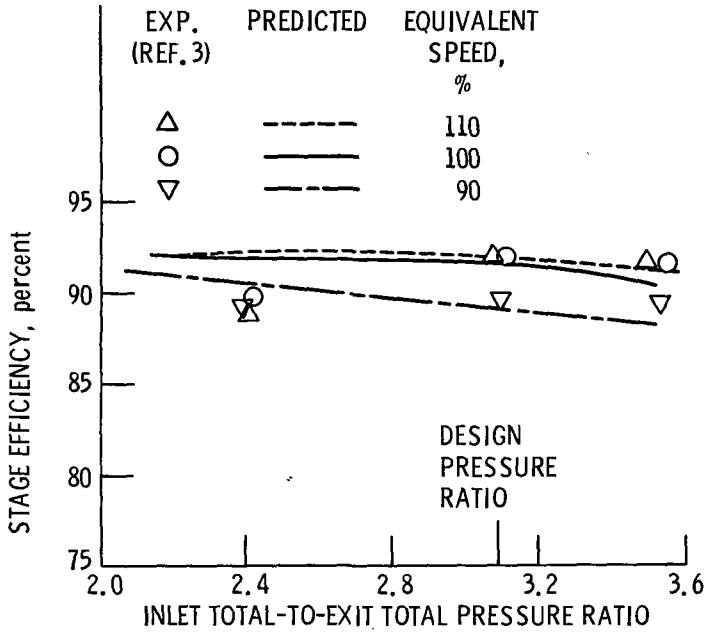

Figure 5. - Comparison of measured and predicted efficiencies for stage 42 A.

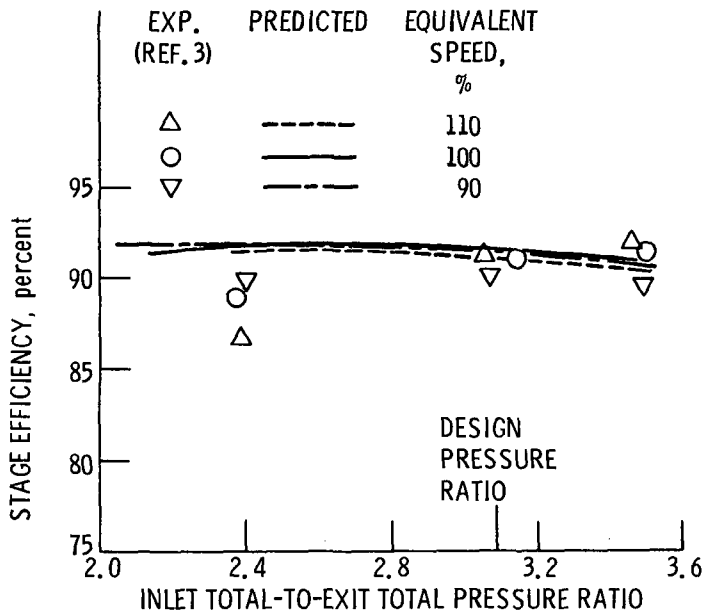

Figure 6. - Comparison of measured and predicted efficiencies for stage 42B.

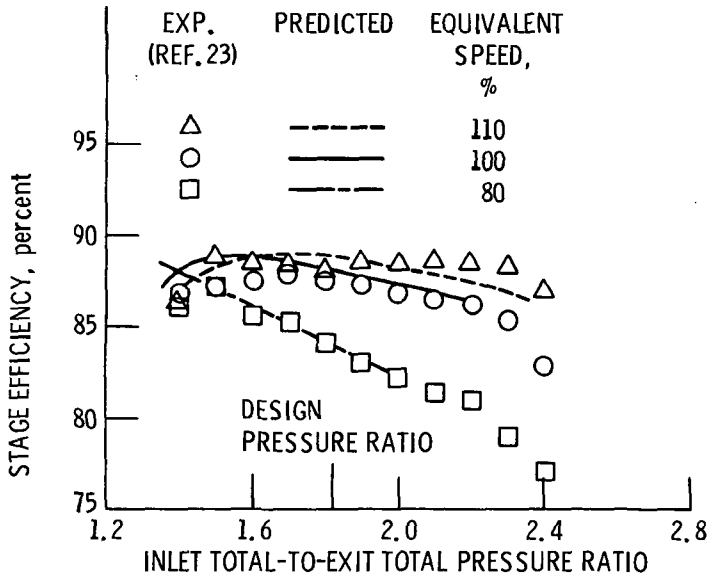

Figure 7. - Comparison of measured and predicted stage efficiency for stage 25U.

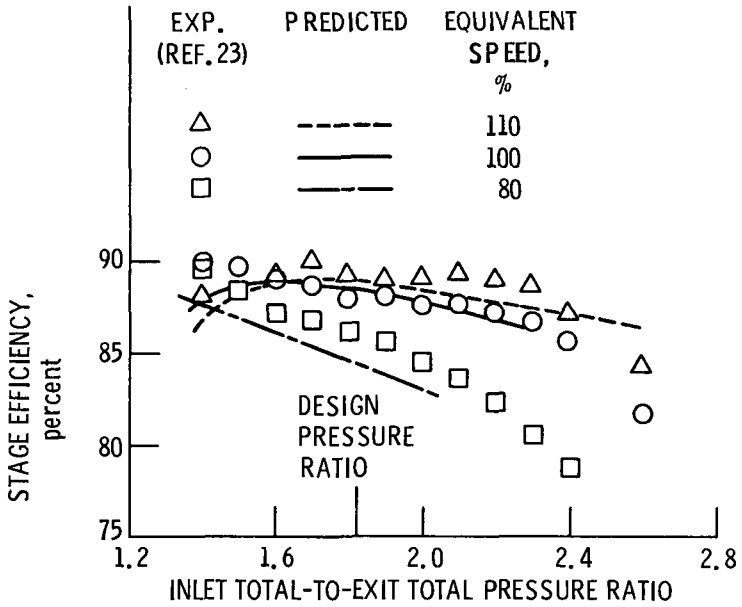

Figure 8. - Comparison of measured and predicted stage efficiency for stage 25 T.

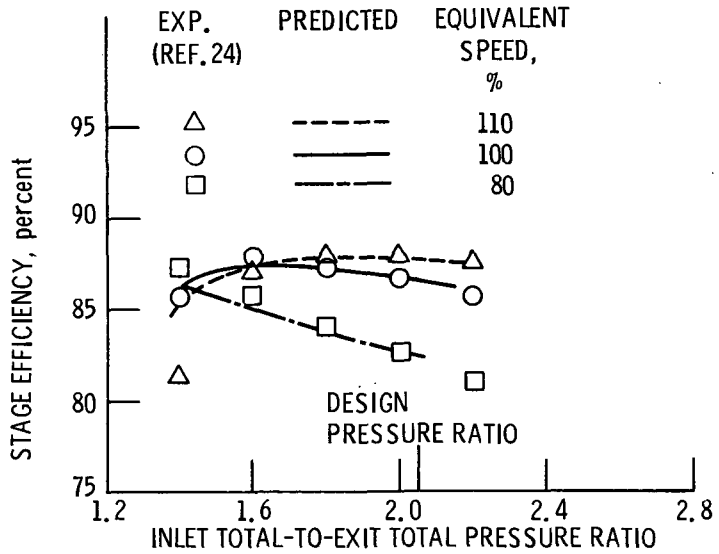

Figure 9. - Comparison of measured and predicted stage efficiency for stage 12.

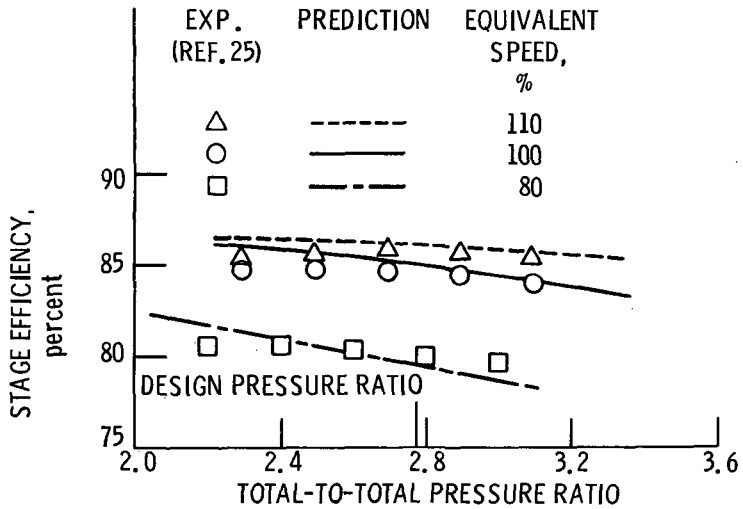

Figure 10. - Comparison between measured and predicted stage efficiency for turbine stage 13 cyl.

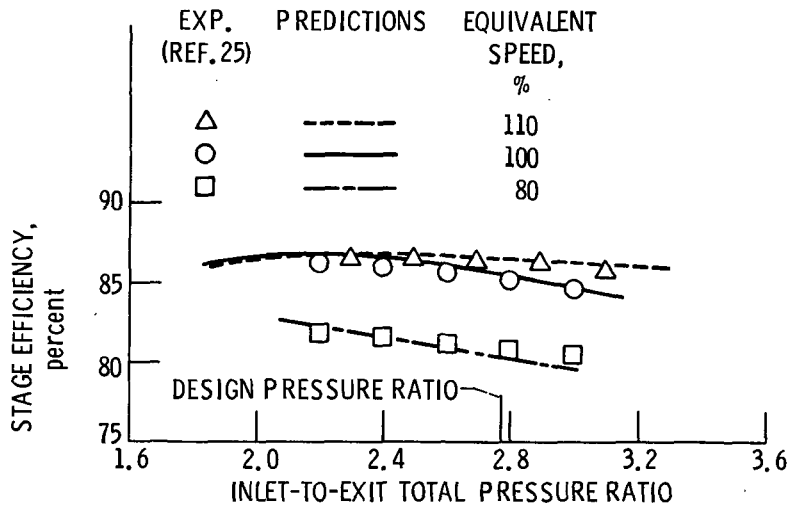

Figure 11. - Comparison between measured and predicted stage efficiency for turbine stage 13-Cone.

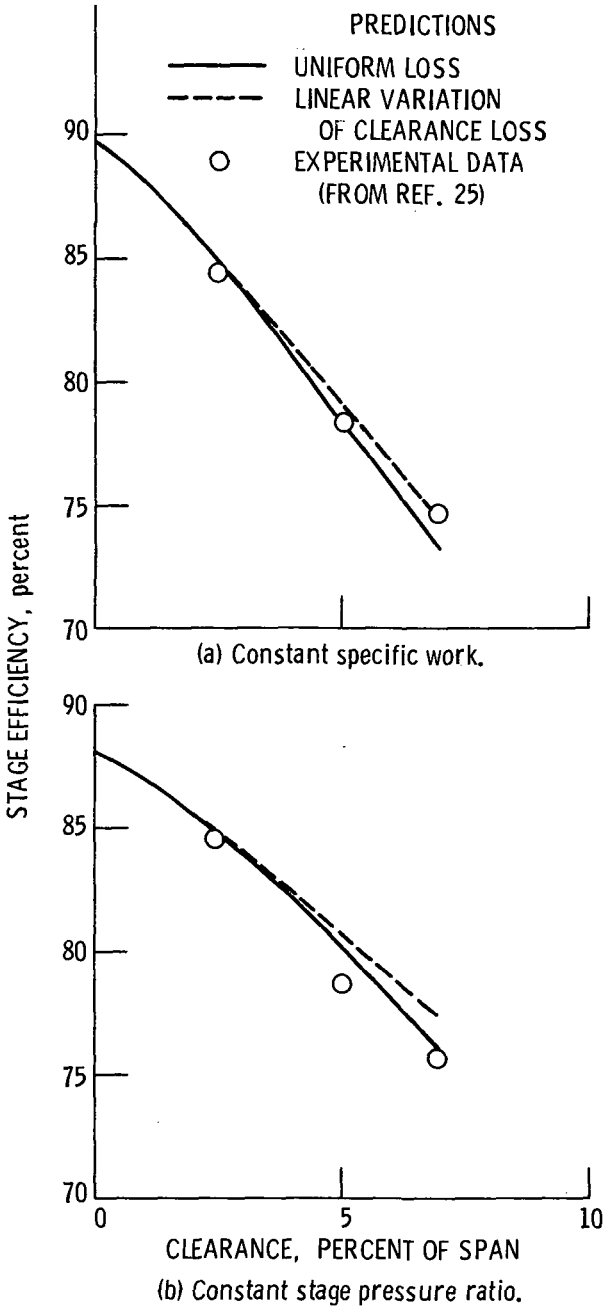

Figure 12. - Comparison between measured and predicted stage efficiency at different clearances for stage 13-cyl.

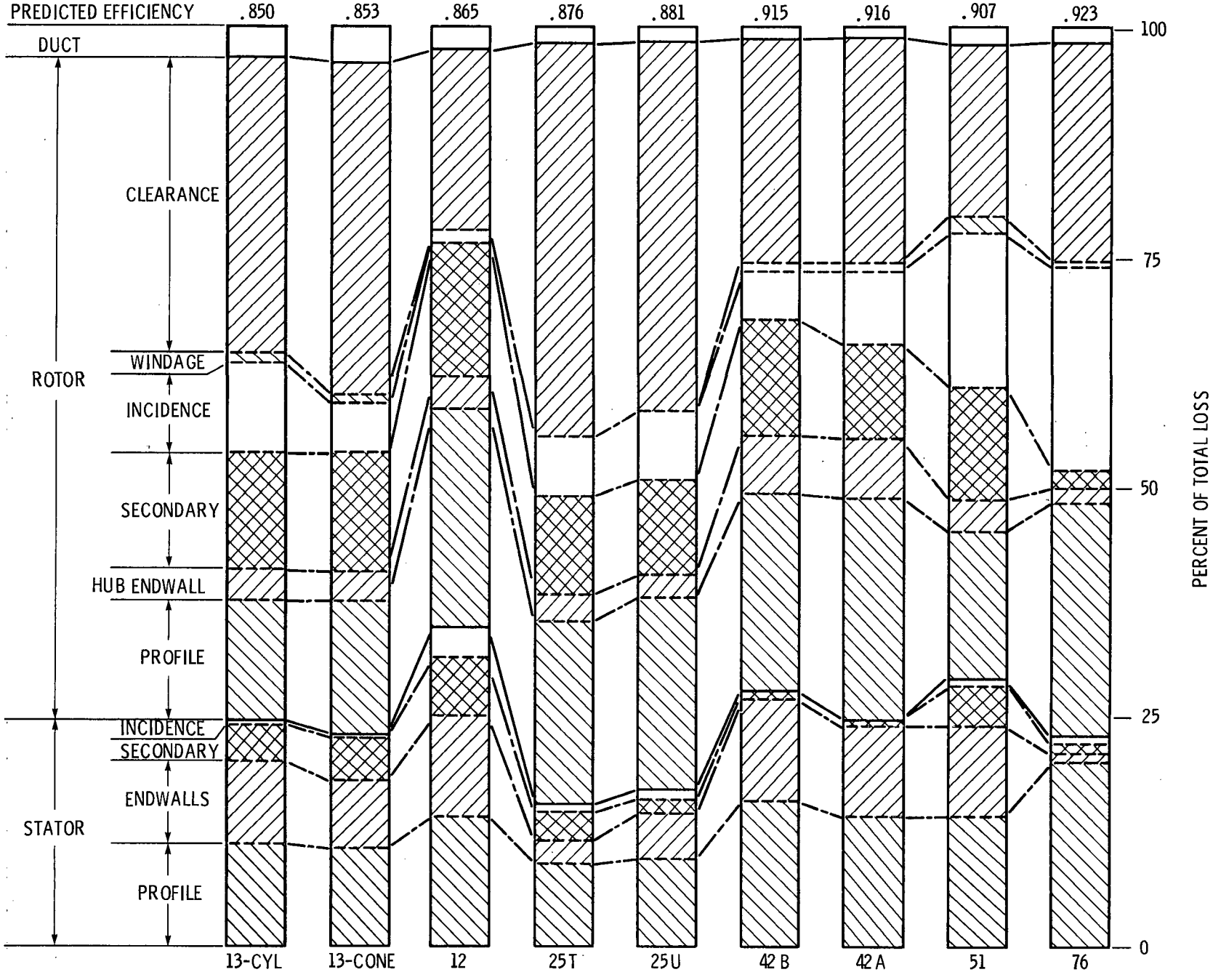

Figure 13. - Loss distribution for each stage at design condition.

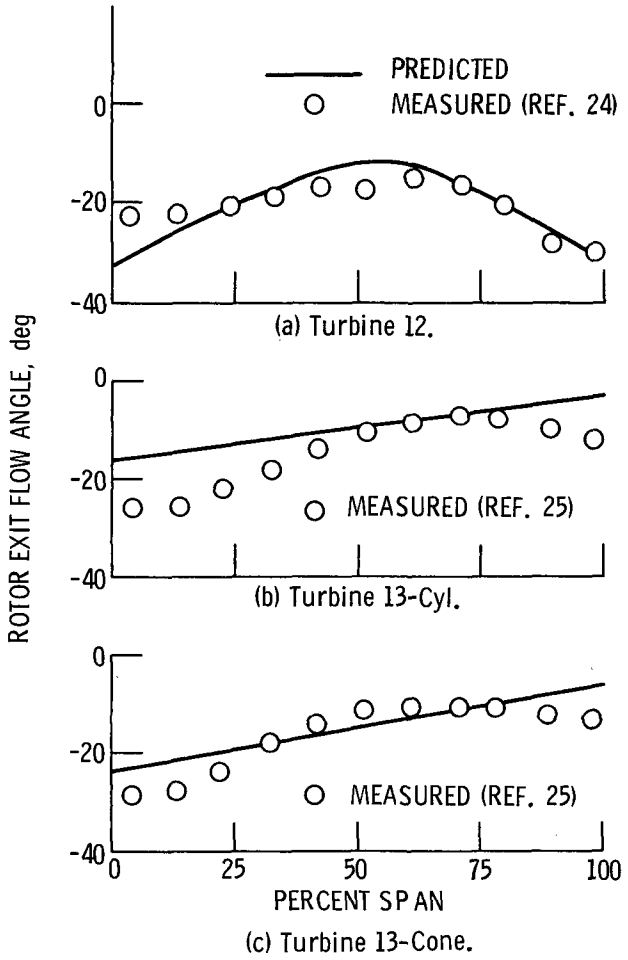

Figure 14. - Comparison of measured and predicted rotor exit flow angles for three turbines at the design point.

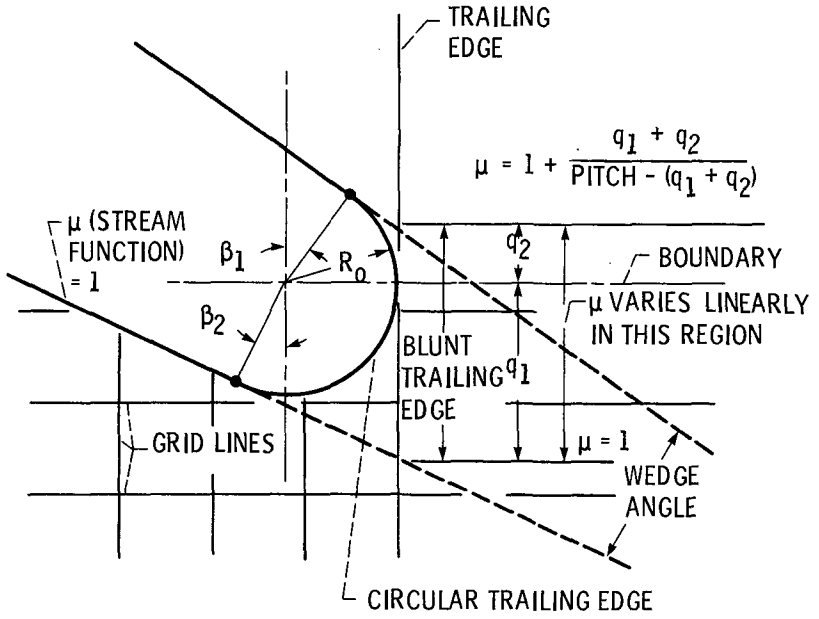

Figure 15. - Schematic of procedure used for trailing edge ejection.

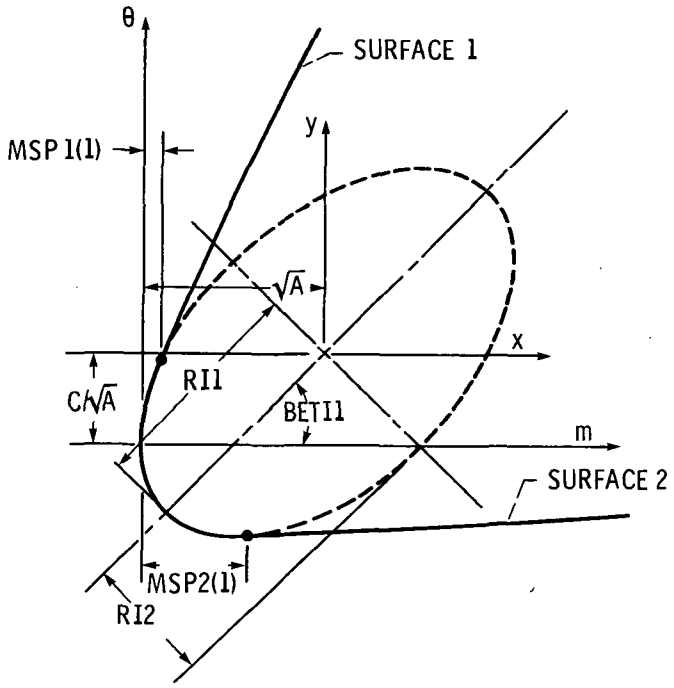

Figure 16. - Schematic of nomenclature used for elliptical blade leading edge.

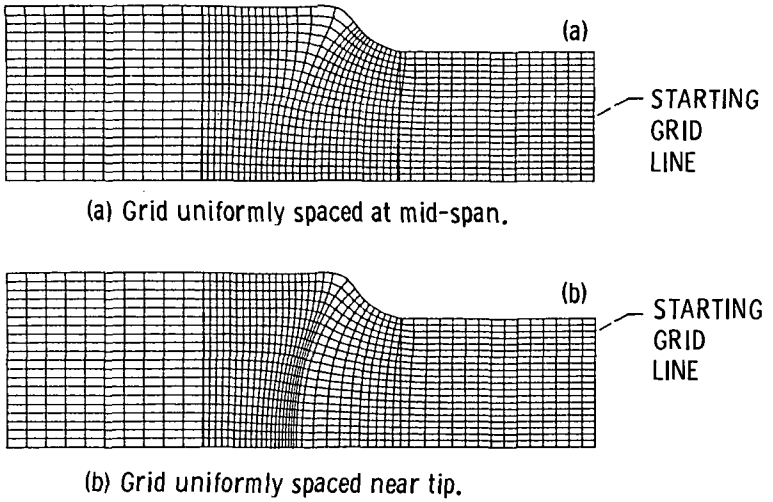

(a) Grid uniformly spaced at mid-span.

(b) Grid uniformly spaced near tip.

Figure 17. - Comparison of grids generated starting at different spanwise locations.

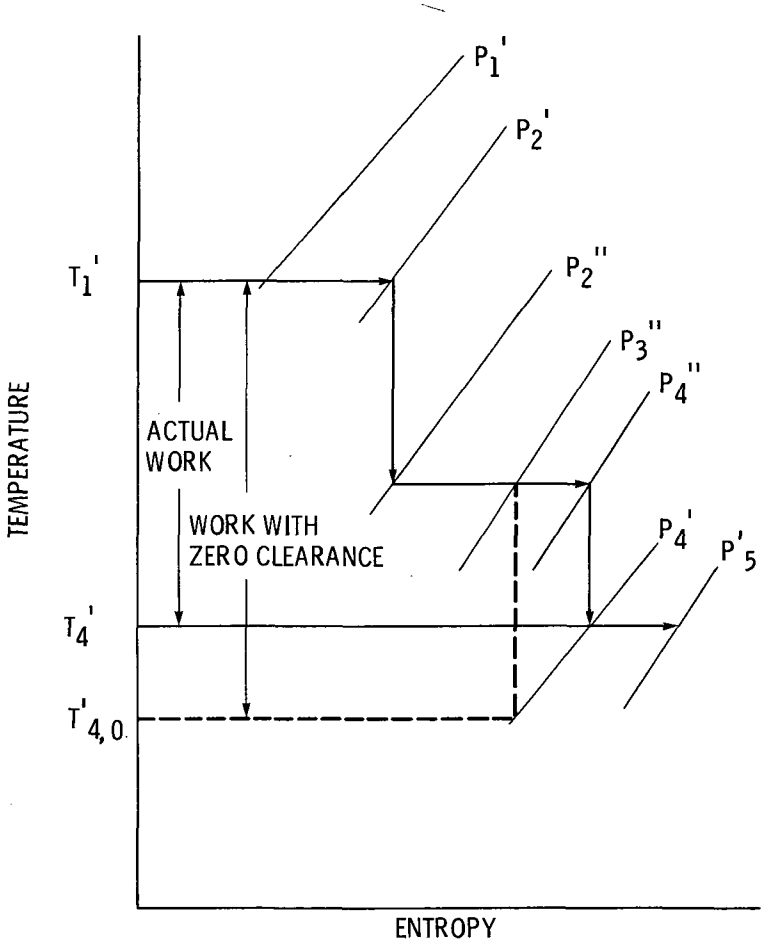

Figure 18. - Sketch of path used to determine stage efficiency.

1. Report No. TM-83640 AVRADCOM TR 84-C-6	2. Government Accession No.	3. Recipient's Catalog No.
4. Title and Subtitle Comparison Between Measured Turbine Stage Performance and the Predicted Performance Using Quasi-3D Flow and Boundary Layer Analyses		5. Report Date 6. Performing Organization Code 535-05-12
7. Author(s) Robert J. Boyle, Jeffrey E. Haas, and Theodore Katsanis		8. Performing Organization Report No. E-2065 10. Work Unit No.
9. Performing Organization Name and Address NASA Lewis Research Center and AVRADCOM Research and Technology Laboratories Cleveland, Ohio 44135		11. Contract or Grant No. 13. Type of Report and Period Covered Technical Memorandum
12. Sponsoring Agency Name and Address National Aeronautics and Space Administration Washington, D.C. 20546 and U.S. Army Aviation Research and Development Command, St. Louis, Mo. 63166		14. Sponsoring Agency Code

15. Supplementary Notes

Robert J. Boyle, Lewis Research Center; Jeffrey E. Haas, Propulsion Laboratory, ABRADCOM Research and Technology Laboratories, NASA Lewis Research Center; Theodore Katsanis, Lewis Research Center. Prepared for the Twentieth Joint Propulsion Conference cosponsored by the AIAA, SAE, and ASME, Cincinnati, Ohio, June 11-13, 1984.

16. Abstract

A method for calculating turbine stage performance is described. The usefulness of the method is demonstrated by comparing measured and predicted efficiencies for nine different stages. Comparisons are made over a range of turbine pressure ratios and rotor speeds. A quasi-3D flow analysis is used to account for complex passage geometries. Boundary layer analyses are done to account for losses due to friction. Empirical loss models are used to account for incidence, secondary flow, disc windage, and clearance losses.

17. Key Words (Suggested by Author(s))	18. Distribution Statement
Performance prediction Gas turbines Efficiency	Unclassified - unlimited STAR Category 07

19. Security Classif. (of this report)	20. Security Classif. (of this page)	21. No. of pages	22. Price*
Unclassified	Unclassified		

*For sale by the National Technical Information Service, Springfield, Virginia 22161

National Aeronautics and
Space Administration

Washington, D.C.
20546

Official Business
Penalty for Private Use, $300

SPECIAL FOURTH CLASS MAIL
BOOK

Postage and Fees Paid
National Aeronautics and
Space Administration
NASA-451

NASA

POSTMASTER: If Undeliverable (Section 158
Postal Manual) Do Not Return